SPE · AAPG · SEG
CCUS
Carbon Capture, Utilization, and Storage

CCUS: 4433269

Forecasting Injection-Induced Fault Reactivation Using Elastic Weakening and Slip-Tendency Indicators During CO_2 Injection

Godsway Akpabli[1*], Hamid Rahnema[1], Kojo Acheampong Boateng[1], Audrey Ayensigna[1], Emmanuel Agyei[1]

Petroleum and Natural Gas Engineering, New Mexico Institute of Mining and Technology, Socorro, NM, United States

Copyright 2026, Carbon Capture, Utilization, and Storage conference (CCUS) DOI 10.15530/ccus-2026-4433269

This paper was prepared for presentation at the Carbon Capture, Utilization, and Storage conference held in The Woodlands, TX, 30 March – 01 April.

The CCUS Technical Program Committee accepted this presentation on the basis of information contained in an abstract submitted by the author(s). The contents of this paper have not been reviewed by CCUS and CCUS does not warrant the accuracy, reliability, or timeliness of any information herein. All information is the responsibility of, and, is subject to corrections by the author(s). Any person or entity that relies on any information obtained from this paper does so at their own risk. The information herein does not necessarily reflect any position of CCUS. Any reproduction, distribution, or storage of any part of this paper by anyone other than the author without the written consent of CCUS is prohibited.

Abstract

Injection-induced seismicity poses a significant risk to the safe and sustainable deployment of geo-energy technologies such as Carbon Capture and Storage (CCS) and geothermal systems. The objective of this study is to develop a laboratory-based experimental framework for forecasting fault reactivation using acoustic, elastic, and mechanical indicators derived from controlled CO_2 injection. The scope focuses on identifying seismic and geomechanical precursors to fault instability under realistic stress conditions relevant to subsurface injection operations.
Hydromechanical acoustic experiments were conducted under true triaxial stress conditions while continuously monitoring time lapse ultrasonic wave velocities during controlled CO_2 injection. P-wave and S-wave velocities were used to quantify changes in elastic properties, anisotropy, and acoustic impedance, while fault activation metrics including slip tendency and Coulomb failure stress were evaluated to assess mechanical stability.

The experiments reveal a sharp transition from stable sliding to stick-slip behavior when pore pressure exceeds 8.5–9.2 MPa, corresponding to a critical shear to effective normal stress ratio of approximately $\tau/\sigma'_n \approx 0.83$. P-wave velocity decreases systematically from approximately 3670 m/s under fully brinesaturated conditions to about 3280 m/s at lower brine saturations, indicating injection-induced elastic weakening. In contrast, S-wave velocities show modest increases and directional divergence, reflecting stress path dependent deformation and evolving elastic anisotropy. These changes result in reduced elastic stiffness and increasingly negative seismic reflection coefficients. The progressive reduction in effective normal stress and increase in shear stress on favorably oriented fault planes lead to monotonic increases in

slip tendency and Coulomb failure stress, with critical thresholds exceeded within a narrow pressure window.
This study provides the first experimentally constrained framework that directly links time-lapse ultrasonic seismic responses to fault reactivation thresholds during CO_2 injection under true-triaxial stress conditions. By demonstrating that elastic weakening and effective stress redistribution alone can robustly forecast fault instability, the work establishes a physics-based methodology for early warning of injectioninduced seismicity and for defining safer operational pressure limits in CCS and other geo energy applications.

Introduction

The rapid increase in atmospheric carbon dioxide concentrations is primarily driven by the combustion of fossil fuels, alongside emissions from hydrocarbon related activities and industrial processes. These anthropogenic sources release large volumes of CO_2 into the atmosphere, contributing significantly to global warming and climate change (Akpabli et al.,2025,Nunes, 2023). Recent global carbon budget assessments indicate that approximately 30 billion metric tons of CO_2 are added to the atmosphere each year, underscoring the scale of the challenge and the urgency of effective mitigation strategies (Friedlingstein et al., 2022). In response to these emissions, subsurface geo-energy technologies such as Carbon Capture and Storage (CCS) and geothermal energy have emerged as critical components of global decarbonization efforts. However, fluid injection associated with these technologies perturbs subsurface stress conditions and pore pressure, potentially reactivating pre-existing faults (Yeboah et al.,2025). While injection-induced seismicity has been documented in numerous field settings, forecasting the onset of fault slip remains challenging due to the complex coupling between fluid flow, elastic property evolution, and fault friction (Boison et al., 2024; Boison et al., 2025, Bodi et al.,2025).
Laboratory experiments provide a controlled environment in which these coupled processes can be directly observed and quantified. Acoustic emission (AE) monitoring and ultrasonic velocity measurements have been shown to be particularly effective for tracking elastic weakening, damage accumulation, and slip nucleation prior to macroscopic fault failure (Lockner, 1993; Ohnaka, 1996). Building on prior geochemical and storage-focused studies in the San Juan Basin, this work presents an experimental framework that integrates laboratory measurements of acoustic velocities, elastic stiffness, impedance contrasts, and AE characteristics to forecast fault activation during CO_2 injection. By linking injection induced elastic weakening and acoustic precursors to fault reactivation thresholds, the framework complements existing geochemical assessments and addresses a critical gap in the mechanical evaluation of CCS-induced seismic risk.

Experimental Methods

A horizontal core plug from the Entrada Sandstone formation, measuring 1.5 inches in diameter and approximately 3 inches in length, was used for the experiments to represent reservoir relevant conditions. The core was oven-dried to a constant mass to remove residual moisture and then fully saturated with a synthetic brine prepared at a salinity of 16,601 ppm based on historical formation water data. Saturation was achieved using a vacuum assisted imbibition procedure to ensure complete pore filling and eliminate trapped air. The saturated core was mounted in a rubber sleeve and placed inside a high pressure core holder connected to a laboratory injection system consisting of displacement pumps, an overburden fluid system, a back-pressure pump, a calibrated burette, and an oven for temperature control. Experiments were conducted at an oven temperature of 94 °C, with an applied overburden pressure of 7,127 psi and a downstream pore pressure of 3,429 psi. The core material had a bulk density of 2,408 kg/m³, a porosity of 9.3%, and an absolute permeability of 0.17 mD, with a pressure drop of 250 psi imposed during absolute permeability measurements. The brine viscosity under experimental conditions was 0.306 cP. This setup enabled controlled fluid injection while maintaining constant stress, pressure, and temperature conditions representative of the Entrada Formation, providing a reliable basis for evaluating flow, acoustic, and

mechanical responses during CO_2 injection experiments.CO_2 was injected continuously at a constant flow rate of 0.02 mL/min under steady-state conditions. Pore pressure, pressure differential across the sample, and injection rate were monitored throughout the experiment. Acoustic velocities were measured periodically during CO_2 injection to capture time-lapse elastic property changes. Ultrasonic P-wave and S-wave velocities were measured during progressive brine displacement by CO_2.

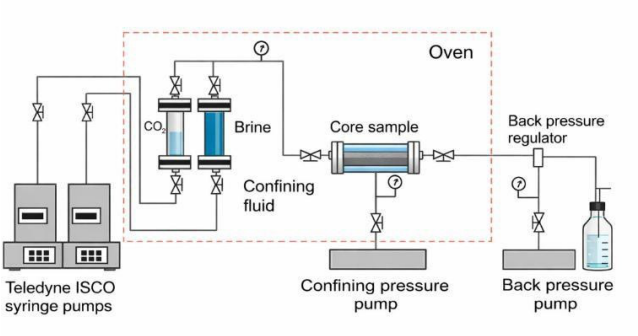

Figure 1: Core flooding system used for the rate CO2 injection test

Results

Measured P-wave velocity decreased systematically as CO_2 displaced brine, while shear-wave velocities exhibited a modest increase. This divergence indicates elastic weakening dominated by fluid substitution effects rather than purely mechanical compaction. The constrained modulus decreased by approximately 20–25% over the course of injection, while shear stiffness increased slightly, reflecting stress-path and fabric effects.

Table 1: Gathered data during the measurements

Day	Saturation (–)	Vp (m/s)	Vs1 (m/s)	Vs2 (m/s)
5/9/2024	1	3674	2772	2804
5/16/2024	0.88	3663	2791	2822
5/24/2024	0.81	3586	2832	2876
6/3/2024	0.73	3397	2868	2926
6/5/2024	0.65	3298	2880	2951
6/10/2024	0.59	3282	2917	2977

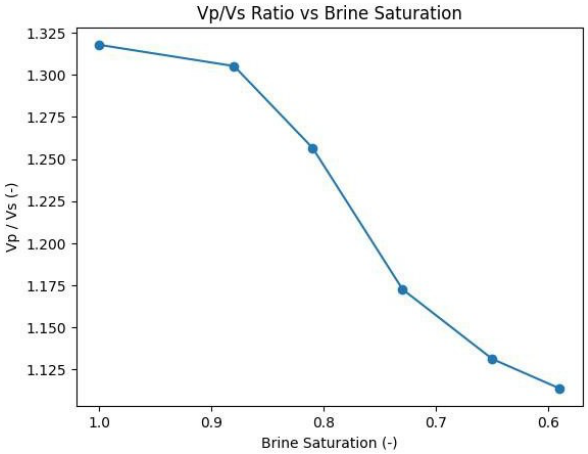

Figure 1: Evolution of the Vp/Vs ratio as a function of brine saturation during CO_2 drainage. The systematic decrease in Vp/Vs reflects elastic weakening driven by fluid substitution and enhanced poroelastic stress transfer. The most pronounced reduction occurs at low brine saturation, coinciding with the pressure range associated with increasing fault slip tendency.

The plots below show P-wave velocity decreases systematically with decreasing brine saturation, reflecting its strong sensitivity to pore fluid properties and fluid bulk modulus, while S-wave velocity remains relatively constant or shows a slight increase because it is primarily controlled by the stiffness of the rock framework. This contrasting behavior indicates that fluid saturation changes mainly affect compressional wave propagation, whereas shear waves respond more to effective stress variations. As a result, the Vp/Vs ratio decreases with decreasing brine saturation, providing a useful seismic indicator for tracking fluid saturation and stress evolution in reservoir rocks.

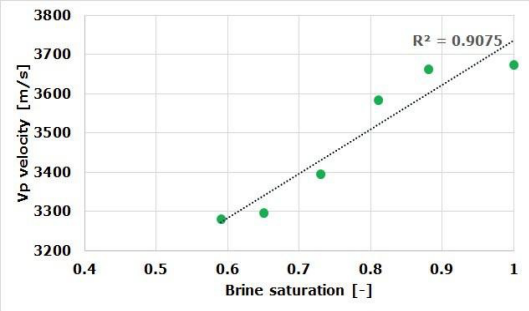

Fig. 3. P-wave velocity as a function of brine saturation.

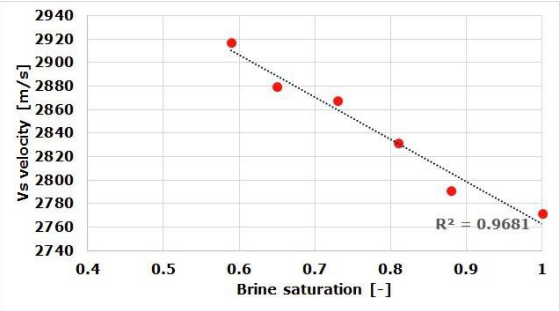

Fig. 4. S-wave velocity as a function of brine saturation

Day	Sw (from Data)	P(t) [MPa]	ΔP [MPa]	σn(t) [MPa]	τ(t) [MPa]	σn'(t) [MPa]	Ts(t)	CFS(t) [MPa]	Activated? (Ts≥μ)	Activated? (CFS≥0)	Ts ≥ 0.83?	P in [8.5,9.2]?
5/9/2024	1.00	7.500	0.000	8.587	1.151	2.587	0.445	-0.401	NO	NO	NO	NO
5/16/2024	0.88	8.300	0.800	8.587	1.151	1.947	0.591	-0.017	NO	NO	NO	NO
5/24/2024	0.81	8.600	1.100	8.587	1.151	1.707	0.674	0.127	YES	YES	NO	YES
6/3/2024	0.73	8.900	1.400	8.587	1.151	1.467	0.785	0.271	YES	YES	NO	YES
6/5/2024	0.65	9.300	1.800	8.587	1.151	1.147	1.004	0.463	YES	YES	YES	NO
6/10/2024	0.59	9.600	2.100	8.587	1.151	0.907	1.269	0.607	YES	YES	YES	NO

Figure 2:presents a time-dependent fault stability assessment in which injection pressure, resolved stresses, slip tendency, and Coulomb failure stress are evaluated to identify the onset of fault reactivation under increasing pore pressure.

Discussion

The experimental results show that injection induced fault activation is systematically preceded by measurable changes in elastic properties and stress-based stability metrics. Progressive reductions in Pwave velocity and acoustic impedance indicate elastic weakening associated with CO_2 invasion and enhanced poroelastic stress transfer. These changes lead to a reduction in effective normal stress on the fault and a corresponding increase in slip tendency. The evolution of impedance contrasts and slip tendency reveals a narrow pressure interval over which critical stability thresholds are exceeded, with fault activation identified at a slip tendency of approximately $T_s \approx 0.83$. Importantly, these elastic and stress based indicators emerge prior to macroscopic fault slip, demonstrating their value for forecasting fault reactivation and informing operational pressure limits. Together, the results establish a physics based framework for predicting and mitigating injection induced fault activation using seismic derived elastic properties and effective stress analysis.

Conclusions

CO_2 injection leads to systematic elastic weakening, manifested by progressive reductions in P-wave velocity, constrained modulus, and acoustic impedance. Together, these results demonstrate that the proposed experimental framework enables physics-based forecasting and mitigation of injection-induced seismicity using laboratory measurements and monitoring data alone.

References

Akpabli, G., Koranteng, D. O., Esmaeilpour, S., & Rahnema, H. (2025, June). Assessing Feasibility and Design for a Geothermal District Heating and Cooling System at New Mexico Tech's Mineral Science and Engineering Complex. In *ARMA US Rock Mechanics/Geomechanics Symposium* (p. D021S016R002). ARMA.

Boison, P.K.N., Ampomah, W., Simmons, J., and Bui, D. 2024. Integrated Geochemical Modeling for CO_2 Sequestration in the San Juan Basin, New Mexico. Paper SPE-221374-MS presented at the SPE Eastern Regional Meeting, Wheeling, West Virginia, USA, October 2024. https://doi.org/10.2118/221374-MS.

Boison, P.K., Ampomah, W., Simmons, J.D., Bui, D., Sibaweihi, N., Amosu, A., and Duartey, K.O. 2025. Geochemical Assessment of Long-Term CO_2 Storage from Core- to Field-Scale Models. **Energies** 18(15): 4089. https://doi.org/10.3390/en18154089.

Lockner, D. 1993. The role of acoustic emission in the study of rock fracture. Journal of Geophysical Research 98(B3): 475–485.https://doi.org/10.1016/0148-9062(93)90041-B

Ohnaka, M. Earthquake cycles and physical modeling of the process leading up to a large earthquake. Earth Planet Sp **56**, 773–793 (2004). https://doi.org/10.1186/BF03353085

Yeboah, N. N., Ampomah, W., Bratton, T., Bui, D., & Amosu, A. (2025, April). Evaluating the impact of stressinduced changes on caprock integrity in the San Juan Basin. In SPE/AAPG/SEG Carbon, Capture, Utilization, and Storage Conference and Exhibition (p. D011S007R001). SPE.

Aki, K., and Richards, P. G., 2002, Quantitative Seismology, University Science Books.

Jaeger, J. C., Cook, N. G. W., and Zimmerman, R., 2007, Fundamentals of Rock Mechanics, Blackwell.

Mavko, G., Mukerji, T., and Dvorkin, J., 2009, The Rock Physics Handbook, Cambridge University Press.https://doi.org/10.1017/9781108333016

Bodi, Vida Ama, Ampomah, William, Bui, Dung, and Najmudeen Sibaweihi. "Assessment of CO_2 Sequestration in a

Stack Storage Complex in the San Juan Basin, NM." Paper presented at the SPE Oklahoma City Oil and Gas Symposium, Oklahoma City, Oklahoma, USA, April 2025. doi: https://doi.org/10.2118/224355-MS

APPENDIX

Table 1. Equations used for elastic, seismic, and faultstability analysis

No.	Quantity	Equation
Eq. (1)	Constrained (P-wave) modulus	$M = \rho V_p^2$
Eq. (2)	Shear modulus	$G = \rho V_s^2$
Eq. (3)	Effective normal stress	$\sigma_n' = \sigma_n - \alpha P$
Eq. (4)	Slip tendency	$T_s = \frac{\tau}{\sigma_n'}$
Eq. (5)	Acoustic impedance	$I = \rho V_p$
Eq. (6)	Reflection coefficient	$R = \frac{I_2 - I_1}{I_2 + I_1}$
Eq. (7)	Shear-wave anisotropy	$A_s = \frac{V_{s2} - V_{s1}}{V_{s,avg}}$
Eq. (8)	Coulomb Failure Stress	$CFS = \tau - \mu\sigma_n'$
Eq. (9)	Critical pore pressure	$P_{crit} = \frac{\sigma_n - \tau/\mu}{\alpha}$

Elastic properties governing stress redistribution during CO_2 injection were derived from ultrasonic velocity measurements and bulk density. The constrained (P-wave) modulus characterizes the compressional stiffness of the rock under undrained conditions and was calculated from the measured Pwave velocity and bulk density, reflecting the combined influence of the rock frame and pore fluid on compressional deformation (Eq. 1). The shear modulus represents the rigidity of the rock framework against shear deformation and was computed using the measured shear-wave velocity and bulk density, providing a measure of the load-bearing skeleton independent of pore fluid compressibility (Eq. 2).

To account for stress-induced elastic anisotropy, directional shear moduli were evaluated using orthogonally polarized shear-wave velocities. The degree of shear-wave anisotropy was quantified by the normalized difference between the two orthogonal shear-wave velocities, providing insight into stresspath-dependent deformation and evolving fabric during injection (Eq. 7).

Fault stability was assessed using effective stress concepts. The effective normal stress acting on the fault plane was calculated by subtracting the pore pressure, scaled by the Biot coefficient, from the total normal stress. This formulation captures the reduction in fault-clamping stress due to increasing pore pressure during injection (Eq. 3). Slip tendency was then defined as the ratio of resolved shear stress to effective

normal stress, serving as a dimensionless indicator of proximity to frictional failure (Eq. 4).

Seismic reflectivity and elastic contrasts induced by CO_2–brine substitution were evaluated using acoustic impedance, defined as the product of bulk density and P-wave velocity. Changes in acoustic impedance directly reflect elastic weakening and fluid substitution effects (Eq. 5). The normal-incidence reflection coefficient between successive saturation states was computed from the impedance contrast, providing a seismic-scale proxy for tracking stress and stiffness evolution during injection (Eq. 6).

Fault reactivation potential was further quantified using Coulomb Failure Stress, which represents the balance between driving shear stress and frictional resistance on the fault plane. Positive values of Coulomb Failure Stress indicate conditions favorable for slip initiation (Eq. 8). Finally, the critical pore pressure required for fault reactivation was derived by rearranging the Coulomb failure criterion, yielding the pore-pressure threshold at which frictional resistance is overcome for a given stress state and friction coefficient (Eq. 9).